Structural and functional features of Crl proteins and identification of conserved surface residues required for interaction with the RpoS/σS subunit of RNA polymerase.

Paola Cavaliere, Fabienne Levi-Acobas, Claudine Mayer, Frederick A Saul, Patrick England, Patrick Weber, Bertrand Raynal, Véronique Monteil, Jacques Bellalou, Ahmed Haouz, et al.

Structural and functional features of Crl proteins and identification of conserved surface residues required for interaction with the RpoS/σ^S subunit of RNA polymerase

Paola Cavaliere*†, Fabienne Levi-Acobas‡§, Claudine Mayer§□¶, Frederick A. Saul§**, Patrick England§††, Patrick Weber§**, Bertrand Raynal§††, Véronique Monteil*†, Jacques Bellalou‡§, Ahmed Haouz§** and Françoise Norel*†[1]

* Institut Pasteur, Unité de Génétique Moléculaire, Département de Microbiologie, 25 rue du Docteur Roux, 75015 Paris, France

† CNRS ERL3526, rue du Docteur Roux, 75015 Paris, France

‡ Institut Pasteur, Plate-forme de Production de Protéines Recombinantes, Département de Biologie Structurale et Chimie, 25 rue du Docteur Roux, 75015 Paris, France

§ CNRS UMR 3528, rue du Dr. Roux, 75015 Paris, France

□ Institut Pasteur, Unité de Microbiologie Structurale, Département de Biologie Structurale et Chimie, 25 rue du Docteur Roux, 75015 Paris, France

¶ Université Paris Diderot, Sorbonne Paris Cité, Cellule Pasteur, Paris, France.

** Institut Pasteur, Plate-forme de Cristallographie, Département de Biologie Structurale et Chimie, 25 rue du Docteur Roux, 75015 Paris, France

†† Institut Pasteur, Plate-forme de Biophysique Moléculaire, Département de Biologie Structurale et Chimie, 25 rue du Docteur Roux, 75015 Paris, France

[1] To whom correspondence should be addressed. Email: francoise.norel@pasteur.fr Tel: (33) 140613122; Fax: (33) 145688960

ABSTRACT

In many γ-proteobacteria, the RpoS/σ^S sigma factor associates with the core RNA polymerase (RNAP) to modify global gene transcription in stationary phase and under stress conditions. The small regulatory protein Crl stimulates the association of σ^S with the core RNAP in *Escherichia coli* and *Salmonella enterica* serovar Typhimurium (*S*. Typhimurium), through direct and specific interaction with σ^S. The structural determinants of Crl involved in σ^S binding are unknown. Here, we report the X-ray crystal structure of the *Proteus mirabilis* Crl protein (Crl_{PM}) and a structural model for *S*. Typhimurium Crl (Crl_{STM}). Using a combination of *in vivo* and *in vitro* assays, we demonstrated that Crl_{STM} and Crl_{PM} are structurally similar and perform the same biological function. In the Crl structure, a cavity enclosed by flexible arms contains two patches of conserved and exposed residues required for σ^S binding. Among these, charged residues likely to be involved in electrostatic interactions driving Crl-σ^S complex formation were identified. Crl_{STM} and Crl_{PM} interact with domain 2 of σ^S with the same binding properties as with full-length σ^S. These results suggest that Crl family members share a common mechanism of σ^S binding in which the flexible arms of Crl might play a dynamic role.

SUMMARY STATEMENT

The Crl protein binds and activates the σ^S subunit of bacterial RNA polymerase. *In vivo* and *in vitro* studies revealed that the σ^S binding determinants of Crl lie in conserved residues located in a cavity enclosed by flexible arms.

SHORT TITLE

Structural and functional features of Crl

KEY WORDS

RpoS, sigma factor, Crl, RNA polymerase, regulation, *Salmonella*

ABBREVIATIONS

Salmonella enterica serovar Typhimurium, STM; *Proteus mirabilis*, PM; bacterial adenylate cyclase-based two hybrid system, BACTH; Isothermal titration calorimetry, ITC; Surface Plasmon Resonance, SPR; Differential scanning calorimetry, DSC; Analytical Ultracentrifugation AUC

INTRODUCTION

Transcription in bacteria is carried out by a multi-subunit RNA polymerase (RNAP) [1]. When the catalytically active core RNAP ($\alpha 2\beta\beta'\omega$, E) associates with one of several σ factors, the RNAP holoenzyme ($E\sigma$) is directed towards a specific set of promoters, depending on the sigma factor bound [2, 3]. Sigma factors present in cells compete for binding to a limited amount of E [4, 5]. The housekeeping sigma factor, σ^{70}, is the most abundant throughout the growth cycle, and exhibits the highest affinity of all sigma factors for E *in vitro* [4, 5]. At the onset of the stationary phase or in response to specific stress conditions, σ^S (also called σ^{38} or RpoS) starts to accumulate, transcribing genes essential for the general stress response and for stationary phase survival [2, 4-7]. The low concentration and affinity for E of σ^S with respect to σ^{70} represent limiting steps in the competition of σ^S for E binding, and thus, in the expression of *rpoS*-dependent genes [5-7]. Bacteria use different strategies to overcome this obstacle by resorting to regulatory factors such as Rsd, 6S RNA and ppGpp [5]. All these factors act at the expense of $E\sigma^{70}$, thus promoting the formation of alternative holoenzymes such as $E\sigma^S$. Another important regulator that increases σ^S competitiveness is the small protein Crl [8-14]. Contrary to the above mentioned regulators and classical transcriptional factors that bind to DNA, Crl binds directly to σ^S facilitating $E\sigma^S$ formation [9, 13-15]. Kinetic studies have shown that Crl binding to σ^S increases the association rate of σ^S with core RNAP and that the σ^S-Crl complex has a short half-life (about 3 s) [15]. It has been proposed that Crl may help σ^S to adopt a conformation with higher affinity for E.

Previous studies demonstrated that Crl does not interact with σ^{70} and functions as a σ^S-specific RNAP holoenzyme assembly factor [13-15]. However, Crl is not as widespread as σ^S in bacteria, and there are many *rpoS*-containing species that do not possess a *crl* gene [16]. Furthermore, in bacterial species containing both *crl* and *rpoS*, Crl is less conserved at the sequence level than σ^S (percentage of sequence identity ranging from 35 to 90 for Crl and 72 to 100 for σ^S) [16]. It is therefore questionable whether Crl has the same σ^S activation role in all species that contain a *crl* gene. So far, Crl has only been functionally characterized in two closely related bacteria, *Escherichia coli* and *Salmonella enterica* serovar Typhimurium (*S.* Typhimurium) and has the same σ^S-enhancer action in both species [8-15], which is not surprising given the high level of sequence identity between these two heterologous Crl proteins (84 %).

σ^S belongs to the σ^{70}-family of sigma factors [17-19] whose members contain at least two structural domains connected by flexible linkers: domain 2, which binds the promoter –10 element, and domain 4 which binds the –35 element of the promoter. Previous studies have focused on the binding region of σ^S involved in the interaction with Crl. Indeed, using a bacterial two-hybrid system (BACTH), we demonstrated that the fragment encompassing residues 72 to 167 of σ^S domain 2 is the only region involved in the specific interaction with Crl from *Salmonella* [20]. At the sequence level, domain 2 is the most highly conserved domain in the σ^{70}-family [17-19]. A recent work pointed to some residues in σ^S domain 2 that are necessary and sufficient for Crl from *E. coli* to discriminate between σ factors other than σ^S [14]. Regarding Crl, we previously reported that four conserved residues are important for its activity and for σ^S-Crl interaction [16]. However, a Crl three-dimensional structure was not available and this made difficult to understand if the identified residues belong to the same region in the structure and if they are exposed and available for interaction with σ^S. Recently, the crystal structure of Crl from *Proteus mirabilis* (Crl_{PM}) was released in the Protein data Bank (PDB 3RPJ, unpublished), providing an important contribution to the comprehension of the Crl structure-function relationships. However, Crl_{PM} has not been functionally characterized and Crl from *P. mirabilis* and from *S.* Typhimurium (Crl_{STM}) share only 47 %

sequence identity, which might result in local structural differences important for their biological function.

Many issues remain to be addressed concerning the Crl-σ^S partnership and its biological function, among which: whether Crl proteins have the same σ^S-activator function and σ^S binding region in various bacterial species, what is the region of Crl involved in the direct interaction with σ^S and what are the determinants that drive the σ^S-Crl complex formation and its fast dissociation rate. To gain insight into the above questions, we solved the crystal structure of Crl_{PM}, modeled the structure of Crl_{STM}, and performed functional analyses of both proteins *in vitro* and *in vivo*. Our data demonstrated that Crl_{STM} and Crl_{PM} display similar structural properties in solution and the same σ^S-enhancer activity, suggesting a common functionality in Crl family members. We further studied the interaction of Crl_{STM} and Crl_{PM} with $\sigma^S{}_{STM}$ and its domain 2 alone, showing that σ^S domain 2 possesses the same binding parameters as full-length σ^S and that no other domains take part in the transient formation of the σ^S-Crl complex. Finally, combined analyses of the Crl_{PM} X-ray crystal structure obtained in this study and the effects of *crl* mutations in *in vivo* and *in vitro* assays, located a cavity enclosed by flexible loops in the Crl structure, in which conserved and exposed residues important for the interaction with σ^S were identified.

MATERIAL AND METHODS

Bacterial strains, bacteriophage, plasmids and growth conditions

Strains and plasmids used in this study are listed in Supplementary Table S1. Bacteriophage P22HT105/1*int* was used to transfer mutations between *Salmonella* strains by transduction [21]. Green plates, for screening for P22-infected cells or lysogens, were prepared as described previously [22]. Strains were routinely grown in Luria-Bertani (LB) medium [23] at 37°C under aeration. Development of the rdar morphotypes was observed on CR plates (LB agar without NaCl supplemented with Congo red 40 μg/ml and Coomassie brilliant blue R250 20 μg/ml), at 28°C as described [11]. Antibiotics were used at the following concentrations: ampicillin (Ap) 100 μg/mL; carbenicillin (Cb) 100 μg/mL; chloramphenicol (Cm) 15 μg/mL for the chromosomal resistance gene and 30 μg/mL for the plasmid resistance gene; kanamycin (Km) 50 μg/mL; and tetracycline (Tet) 20 μg/mL.

crl allelic exchange in *Salmonella*

Allelic exchange of *crl* in *S*. Typhimurium ATCC14028 was achieved with a two-step Red-recombinase-based recombineering procedure [24-26]. The procedure involves 1) replacement of the *crl* coding sequence by a *tetRA* module (produced by PCR, Table S2) yielding strain VFD416, and 2) replacement of the *tetRA* module by a PCR-amplified DNA fragment (Table S2) of the *crl* allele from pVFB430, pVFD49 and VFC362 through positive selection of tetracycline-sensitive recombinants. All strains were confirmed to contain the expected mutation by DNA sequencing.

BACTH analyses

The bacterial adenylate cyclase-based two hybrid (BACTH) assay is dependent upon the functional reconstitution of the *Bordetella pertussis* adenylyl cyclase T18 and T25 sub-domains by two interacting partners [27]. The resulting cyclic AMP binds to and activates the transcription activator CRP, a positive regulator of the *lac* and *mal* operons involved in lactose and maltose catabolism. The *E. coli cya* strain DHT1 was transformed with derivatives of plasmids pKT25 and pUT18 encoding σ^S and Crl proteins fused to the C-terminal part of T25 and the N-terminal part of T18, respectively. Co-transformants were plated onto MacConkey maltose plates supplemented with carbenicillin, kanamycin, and 0.5 mM IPTG to assess the Mal phenotype and on LB plates supplemented with X-Gal (40 μg/ml) Cb, Km, and IPTG (0.5 mM) to assess the Lac phenotype. Plates were incubated at 30°C for 2 days and then isolated colonies were grown in LB supplemented with Cb, Km, and IPTG, at 30°C for 20 hours. β-galactosidase activities were measured as described by Miller [28].

ITC and SPR experiments

ITC experiments were carried out at 25°C using a MicroCal VP-ITC microcalorimeter (GE Healthcare) with a cell volume of 1.5 mL. In each titration experiment, volumes of 7-10 μL of a solution containing Crl_{STM} or Crl_{PM} at concentrations of 200-230 μM were injected into a σ^S-containing solution in the same buffer (50 mM Na-phosphate pH 8.0, 300 mM potassium glutamate), using a computer-controlled 250 μL microsyringe. All the σ^S samples were prepared at concentrations of 15-20 μM. SPR binding assays were conducted on a Biacore X100 instrument (GE Healthcare), equilibrated at 25°C in 50 mM Na-phosphate pH 8.0, 300

mM potassium glutamate as previously described [15]. All experiments were performed in triplicate and standard deviations were calculated. For details see Supplementary Material and Methods.

Crystallization and structure determination of recombinant Crl and homology modeling

Initial screening of crystallization conditions was carried out for Crl_{STM} and Crl_{PM} by the vapour diffusion method with a Mosquito^{TM} nanoliter-dispensing system (TTP Labtech). Sitting drops were set up using 400 nL of a 1:1 mixture of each Crl protein and crystallization solutions (672 different commercially available conditions) equilibrated against 150 μL reservoir in multiwell plates (Greiner Bio-One). The crystallization plates were stored at 18°C in a RockImager1000^{TM} (Formulatrix) automated imaging system to monitor crystal growth. Only Crl_{PM} yielded suitable crystals. Manual optimization was performed in Limbro plates by the hanging-drop method. The best crystals were obtained by mixing 1.5 μL of protein at 16.3 mg/mL with 1.5 μL reservoir solution containing 30 % (w/v) PEG3000 and 100 mM CHES-NaOH pH 9.5. Single crystals were flash-cooled in liquid nitrogen using a mixture of 50% Paratone-N and 50% paraffin oil as cryoprotectant. X-ray diffraction data were collected on beamline PROXIMA-1 at Synchrotron SOLEIL (Saint-Aubin, France). The diffraction images were integrated with the program XDS [29] and crystallographic calculations were carried out with programs from the CCP4 program suite [30]. The structure of Crl_{PM} was solved by the molecular replacement method with the program Phaser [31] using PDB entry 3RPJ as a template. Two independent protein molecules were identified in the crystallographic asymmetric unit. The structures were refined by alternate cycles of restrained maximum-likelihood refinement with the program Refmac5 [32] and manual adjustments were made to the models with Coot [33]. TLS refinement was used in the last cycles of refinement, with one TLS group per molecule.
The structure of Crl_{STM} was modeled using the crystal Crl_{PM} structure (chain A of 4Q11) as a template, with the program MODELLER provided by the Bioinformatics Toolkit (http://toolkit.tuebingen.mpg.de/modeller) [34]. The model quality was assessed using the ModFOLD server [35]. The Crl_{STM} model has a global model quality score of 87 % and a P-value $1.07*10^{-4}$. The model spans residues 1 to 133. Structural superpositions were performed using the TM-align server [36]. This model was also validated by a theoretical calculation of the hydrodynamic properties of the crystal structure of Crl_{PM} (4Q11) and the structural model of Crl_{STM}. All structural figures were generated with PyMOL (http://www.pymol.org).

Methods for DNA manipulation and immunoblot analysis of proteins, protein production and purification and DSC, CD, fluorescence and AUC experiments are described in Supplementary Material and Methods.

RESULTS AND DISCUSSION

Structural features of Crl

Crl has been reported to bind σ^S and increase its activity in two closely related species, *S*. Typhimurium and *E. coli* K12 [8-16], but three-dimensional structures for these Crl proteins are not available. The crystal structure of Crl from *P. mirabilis* was solved by the Midwest Center for Structural Genomics consortium (pdb entry 3RPJ; unpublished work), but this protein has not been functionally characterized. Both *P. mirabilis* and *S*. Typhimurium belong to Enterobacteria but their Crl proteins share 47 % sequence identity (Supplementary Figure S1A), which is lower than the 79 % sequence identity shared by their σ^S proteins (Supplementary Figure S1B).

Our attempts to crystallize Crl_{STM} were unsuccessful despite numerous trials under different screening conditions, including seeding with crystals of Crl_{PM}. On the contrary, we obtained crystals of Crl_{PM} under different crystallization conditions and with a different space group ($P2_1$) than the 3RPJ crystal structure ($P2_12_12_1$), and we solved the corresponding structure at 1.95 Å resolution (PDB code 4Q11). The crystal parameters, data statistics, and final refinement parameters are shown in Supplementary Table S3. Two independent monomers are present in the asymmetric unit (Figure 1A). Continuous electron density was seen for residues 7-132 in monomer A and 5-130 in monomer B. The two monomers were superimposed with an rmsd of 0.36 Å for 123 equivalent Cα atoms. Each monomer folds as a single α/β domain containing four α-helices (α2 and α4 are 3_{10} helices), a five-stranded mixed β-sheet and an additional single β-strand with an overall α1α2β1β2β3β4β5α3β6α4 architecture (Figure 1B and Supplementary Figure S1A). In the crystal structure, two types of dimers were observed with interfaces of 685 and 987 $Å^2$, respectively [37]. The first dimer is formed by the two independent monomers (A, B) related by a non-crystallographic two-fold axis between the β5 strands (Figure 1A) and is conserved in the 3RPJ structure. The second dimer (Supplementary Figure S2) is formed by monomer A and a symmetry-equivalent monomer B. Superposition of the two dimeric structures gave rise to an rmsd of 0.42 Å for all equivalent C_α atoms).

Interestingly, the Crl_{PM} structure contains an exposed cavity of approximately 16 Å in length and 8 Å deep enclosed by three flexible loops (loop 1 including residues 22-32, loop 2 including residues 42-52, loop 3 including residues 77-80), and the bottom of the cavity is formed by the β1β2β3 antiparallel β-sheet (Figure 1B). High atomic temperature factor values were observed for loops 1 and 2, suggesting flexibility in these regions (the loop 3 appeared to be less flexible) (Figure 1C). These loops may play a dynamic role in the biological activity of Crl.

Crl_{PM} and Crl_{STM} are monomeric proteins and share similar structural properties in solution

Previous studies using gel filtration analyses [9, 13] suggested that Crl is monomeric in solution. However, since two possible types of Crl_{PM} dimers were observed in the 4Q11 crystal structure and the dimeric form shown in Figure 1A is conserved in the 3RPJ and 4Q11 structures, we explored the possibility of Crl dimer formation in solution. For this purpose, we performed AUC experiments with Crl_{STM} and Crl_{PM} at different concentrations. Both proteins sedimented as single species compatible with a monomeric form at all the concentrations tested (Supplementary Figure S3). This finding is consistent with *in silico* analyses of the oligomerization state using PISA [37] suggesting that the dimers observed in the crystal structures of Crl_{PM} are not stable.

We used additional biophysical techniques to further investigate whether Crl_{STM} and Crl_{PM} adopt similar structures in solution. Far-UV and near-UV CD spectra showed a similar secondary and tertiary content for both Crl proteins (Supplementary Figure S4A,B). Analogously, fluorescence experiments revealed a similar structural arrangement around the tryptophans for both Crl proteins (Supplementary Figure S4C). Interestingly, the maximum of the fluorescence emission for Crl_{PM} presents a blue-shift for both 280 nm and 295 nm excitation, suggesting a more closed structure for Crl_{PM} with respect to Crl_{STM}. DSC experiments were performed to evaluate and compare the thermal stabilities of Crl_{STM} and Crl_{PM}. The DSC thermogram of both Crl proteins displayed a single transition peak (Supplementary Figure S4D) and the thermal denaturation was irreversible (data not shown). The transition temperature for Crl_{STM} was higher than for Crl_{PM}, indicating a higher thermal stability of Crl_{STM} with respect to Crl_{PM}. In contrast, the enthalpy change correlated with the thermal unfolding of Crl_{PM} is higher than Crl_{STM}, suggesting a different arrangement of intra-molecular interactions that stabilize the secondary and tertiary structure of both proteins.

Altogether, these results showed that Crl_{STM} and Crl_{PM} globally adopt a similar secondary and tertiary structure in solution. The small spectral and thermal stability differences observed between the two proteins could result from local structural changes, notably in the flexible loops 1 and 2 and might potentially result in different binding mechanisms and affinities for σ^S.

Crl_{PM} interacts with σ^S and increases its activity *in vivo*

We previously reported the function of Crl and its interaction with σ^S in S. Typhimurium [11, 12, 16, 20], but until now Crl_{PM} had not been characterized. Since differences in the structure and/or sequence of Crl_{PM}, compared to $Crl_{STM,}$ may result in a different recognition mechanism of σ^S, we investigated whether Crl_{PM} was able to bind σ^S using the BACTH system [27]. This assay is based on the functional reconstitution of adenylate cyclase activity using its T18 and T25 fragments and was successfully used to reveal the interaction between a C-terminal fusion of Crl_{STM} to the T18 fragment (Crl_{STM}-T18) of adenylate cyclase and an N-terminal fusion of σ^S_{STM} to the T25 fragment (T25-σ^S_{STM}) of adenylate cyclase [16, 20]. The T25-σ^S_{STM}, T25-σ^S_{PM}, Crl_{STM}-T18 and Crl_{PM}-T18 proteins were used here to assess the efficiency of interactions between homologous and heterologous σ^S and Crl proteins (Figure 2A) and their expression levels were checked by immunodetection using T25 and T18 antibodies (Figure 2B). Crl_{PM} was able to interact with σ^S_{PM}. In addition, despite the low level of sequence identity of the couple Crl_{STM}-Crl_{PM} with respect to σ^S_{STM}-σ^S_{PM}, Crl_{PM} and Crl_{STM} were able to bind σ^S_{STM} and σ^S_{PM}, respectively. Whilst the T18 antibody was able to detect Crl_{STM}-T18 and Crl_{PM}-T18 (Figure 2B), a polyclonal antibody directed against Crl_{STM} was efficient to recognize Crl_{STM}-T18 but not Crl_{PM}-T18 (data not shown), suggesting that the major antigenic determinants located at the surface of Crl_{STM} are not conserved in Crl_{PM}.

In a previous work, we characterized the σ^S_{STM}-Crl_{STM} interaction using surface plasmon resonance [15]. Sigma factors are flexible molecules [38] and dynamic conformational changes might be key features for their function and regulation. Therefore, to assess the possibility that the immobilization of $(his)_6$-σ^S on the sensor chip might affect its binding properties for Crl, we monitored the σ^S_{STM}-Crl_{STM} and σ^S_{STM}-Crl_{PM} interactions in solution by ITC experiments, using a σ^S_{STM} protein without a his-tag (Supplementary Figure S5). Analysis of the isotherms revealed that the stoichiometry of the σ^S-Crl_{STM} and σ^S-Crl_{PM} complex was 1:1 with a K_D value of 0.8 μM for Crl_{STM} and 0.4 μM for Crl_{PM} (Table 1). It is worth noting that the affinity obtained for the interaction of σ^S_{STM} with Crl_{STM} was about three-fold higher than that obtained by SPR ([15] and Figure 3A). Interestingly, the Δ_bH values for

Crl_{STM} and Crl_{PM} binding were similar (Table 1), suggesting that the driving forces for σ^S-Crl complex formation are similar for both Crl proteins. In particular, negative values of enthalpy changes imply that the binding between σ^S and Crl is likely driven by electrostatic interactions, whilst positive values of entropy changes suggest that hydrophobic contacts between the exposed apolar residues on the surface of both proteins might be involved.

The above results showed the ability of Crl_{PM} to recognise and bind σ^S, in a similar manner as Crl_{STM}. To assess whether the interaction between $\sigma^S{}_{STM}$ and Crl_{PM} was functional, i.e. if Crl_{PM} is able to increase σ^S activity *in vivo*, we performed allelic exchange in *S.* Typhimurium in which the *crl* gene was replaced by the *crl* allele from *P. mirabilis*. The ability of Crl_{PM} to activate $\sigma^S{}_{STM}$ was then evaluated by monitoring the development of the rdar morphotype by the recombinant *S.* Typhimurium strain (Figure 4A). Indeed, we previously reported that Crl is required for development of the rdar colony morphology of *S.* Typhimurium [11] caused by the σ^S-dependent production of curli and cellulose and correlated with biofilm formation [39]. In contrast to the Δ*crl* mutant of *S.* Typhimurium, strains harboring the crl_{PM} allele displayed a typical rdar morphotype, indicating that Crl_{PM} was able to increase the activity of $\sigma^S{}_{STM}$.

Domain 2 of σ^S is sufficient for *in vivo* and *in vitro* interaction with Crl proteins

σ^S belongs to the σ^{70}-family [17-19] whose members contain at least two structural domains connected by flexible linkers: σ_2, which binds the promoter –10 element and σ_4 which binds the promoter –35 element (See Supplementary Figure S6A). Both domains also interact with the core RNAP [17-19]. We previously reported that residues 72 to 167 of $\sigma^S{}_{STM}$ domain 2 are sufficient for Crl_{STM}-$\sigma^S{}_{STM}$ interaction in BACTH assays [20]. Consistently, the Crl protein from *E. coli* was recently been shown to interact with domain 2 of σ^S [14]. As Crl_{PM} has a two-fold higher affinity for $\sigma^S{}_{STM}$ than Crl_{STM} (Table 1), it might recognize additional domains of σ^S. The truncated T25-$\sigma^S{}_{STM}$ variants previously used in BACTH assays with Crl_{STM} [20], were used here with Crl_{PM} (Supplementary Figure S6A). The only $\sigma^S{}_{STM}$ fragments interacting with Crl_{PM} were those containing domain 2. All the T25-$\sigma^S{}_{STM}$ constructs had similar expression levels, when evaluated by immunodetection with the T25 antibody (Supplementary Figure S6B). Therefore, residues 72 to 163 in $\sigma^S{}_{STM}$ are sufficient for interaction *in vivo* with Crl_{PM}, analogously as for Crl_{STM} [20].

So far, the only evidence that σ^S domain 2 interacts with Crl is based on experiments in bacterial two hybrid systems [14, 16, 20]. To characterize the *in vitro* interaction of σ^S domain 2 with Crl, a fragment of $\sigma^S{}_{STM}$, comprising residues from 53 to 162 ($\sigma^S{}_{53\text{-}162}$), was purified using a co-expression system with Crl_{STM} (See Supplementary Materials and Methods). This co-expression strategy was adopted for two reasons: i) attempts to purify $\sigma^S{}_{53\text{-}162}$ alone failed as the protein was always found in the insoluble fraction (data not shown) and ii) because we could take advantage of the short life-time of σ^S-Crl complex to purify $\sigma^S{}_{53\text{-}162}$ without Crl. Indeed, to evaluate if $\sigma^S{}_{53\text{-}162}$ was bound to Crl_{STM} or free in solution after purification, a small fraction of the purified protein was loaded onto a Superdex 75 10/300 GL column and then analyzed by immunodetection using His-tag antibody. The results demonstrated that $\sigma^S{}_{53\text{-}162}$ was free in solution and the far-UV CD spectrum confirmed a correct folding of this domain (data not shown). However, at high concentrations, $\sigma^S{}_{53\text{-}162}$ aggregated and only a small percentage of the protein was in a monomeric form in AUC and DSC experiments (data not shown), which prevented us from performing ITC experiments. Therefore, SPR experiments were performed since low concentrations of $(his)_6$-$\sigma^S{}_{53\text{-}162}$ were sufficient to immobilize this protein on the sensor chip through its N-terminal end [15]. SPR experiments were also carried out between the full-length $(his)_6$-$\sigma^S{}_{STM}$ and Crl_{STM}, as a control (Figure 3). In these conditions, $(his)_6$-$\sigma^S{}_{53\text{-}162}$ was able to recognize and bind both Crl_{STM} and

Crl_{PM}, confirming the *in vivo* data. Crl_{PM} showed a two-fold higher affinity for $\sigma^S_{53\text{-}162}$ than Crl_{STM} ($K_{D,app}$ = 3.0 ± 0.4 μM), in agreement with the results obtained for the full-length σ^S in ITC experiments (Supplementary Figure S5).

Furthermore, the interaction of $\sigma^S_{53\text{-}162}$ with Crl_{STM} gave a $K_{D,app}$ value of 7 ± 1 μM, very similar to that one obtained for the full-length σ^S ($K_{D,app}$ = 6.0 ± 0.7 μM). This finding showed for the first time that *in vitro* isolated σ^S domain 2 is sufficient to account for σ^S binding to Crl. Kinetic studies previously showed that σ^S-Crl is a transient complex with a fast dissociation phase [15]. The kinetics of interaction with Crl_{STM} of $\sigma^S_{53\text{-}162}$ appeared to be similar to that of full-length σ^S_{STM}. These results suggested that domain 2 is the only domain of σ^S involved in both association and dissociation of the σ^S-Crl complex.

Conserved residues in the Crl family members are mostly surface exposed

The results above showed that Crl_{PM} and Crl_{STM} interact with domain 2 of σ^S_{STM} with similar binding parameters despite their lower sequence identity with respect to the couple σ^S_{STM}-σ^S_{PM}. Thus, the interaction between σ^S and Crl might occur through either a specific Crl structural recognition motif or conserved residues on the surface of the protein. We previously identified 17 conserved residues in Crl-like proteins including Crl_{STM} and Crl_{PM} (Supplementary Figure S1A) and alanine substitutions of some of these residues were shown to affect σ^S binding in BACTH and/or Crl activity *in vivo* [16]. To localise these residues in the Crl structure and understand the possible effects of mutations, we constructed the structural homology model of Crl_{STM} (Figure 5A) based on our X-ray crystal structure of Crl_{PM} and on the alignment shown in Supplementary Figure S1A. This model was validated by a theoretical calculation of the hydrodynamic properties of the crystal structure of Crl_{PM} (4Q11) and the structural model of Crl_{STM}.

Interestingly, we observed that 80% of the identified conserved residues are surface exposed on the Crl structure. Of the 17 conserved residues, only four are buried inside the structure (Phe^{35}, Gly^{55}, Trp^{56}, Gly^{74}), and three of them were shown to be not required for σ^S_{STM} binding [16]. Indeed, the Ala variants of residues Phe^{35}, Gly^{55} and Gly^{74} gave positive results in BACTH and/or in Crl activity assays. In contrast, the Crl Trp^{56}Ala variant abolished σ^S binding and Crl activity [16]. Trp^{56} form an interaction network with neighbouring hydrophobic residues Tyr^{22}, Tyr^{71} and Phe^{103} (Supplementary Figure S7A) and thus might be important for the overall structural stability of the protein. Therefore, in the following analysis, we focused on the other 13 Crl surface-exposed conserved residues and their possible implication in σ^S binding.

Two patches of conserved and surface exposed residues in Crl are involved in σ^S_{STM} binding

Among these 13 residues, all except one (Glu^{52}) are clustered in three different patches on the same face of the Crl structure (Figure 5B). Glu^{52} is located on the opposite face (Supplementary Figure S7B) and its substitution by alanine did not affect Crl activity and interaction with σ^S [16].

Patch 1 consists of residues Gly^{20}, Pro^{21}, Tyr^{22}, Arg^{24} and Asp^{36}. All residues, with the exception of Asp^{36}, are located in loop 1 (Figure 5C). The Tyr^{22}Ala substitution had a negative effect on σ^S binding in BACTH assays and, to a lesser extent, on Crl_{STM} activity *in vivo* [16]. The side chain of Tyr^{22} is oriented towards the long α2-helix and forms an interaction network with other conserved aromatic residues (Trp^{56} and Phe^{103}), as mentioned above (Supplementary Figure S7A). The alanine substitution of residue Gly^{20} mildly affected the Crl_{STM}-σ^S interaction (Supplementary Figure S8). Residue Asp^{36} is located in the β2 strand

with its side chain oriented towards the center of the cavity and is a likely candidate for interaction with σ^S. Consistent with this hypothesis, the substitution $Asp^{36}Ala$ in Crl abolishes its interaction with σ^S (Figure 4B). Interestingly, residues Asp^{36} and Arg^{24} establish a salt bridge in the 4Q11 crystal structure, but Arg^{24} is unlikely to be directly involved in σ^S binding since the substitution $Arg^{24}Ala$ only slightly affected the Crl_{STM}-σ^S interaction (Figure 4B). Furthermore, the Crl_{STM} $Arg^{24}Ala$-$Asp^{36}Ala$ variant did not interact with σ^S (Figure 4B), excluding the possibility that Asp^{36} is required solely to establish electrostatic interaction with Arg^{24}. Crl_{STM}-T18 variants with alanine substitutions had similar expression levels with respect to wild-type Crl_{STM}-T18 (Figure 4D). Altogether these results suggested that Asp^{36} is a key residue for Crl-σ^S complex formation.

Patch 2 (Cys^{41}, Pro^{48}, Arg^{51} and Phe^{53}) faces patch 1 (Figure 5D) and all residues, except Phe^{53}, are located in loop 2. Alanine substitution of Cys^{41} slightly affected the Crl_{STM}-σ^S interaction (Supplementary Figure S8) and was active *in vivo* [16]. In contrast, the substitutions $Arg^{51}Ala$ and $Phe^{53}Ala$ drastically reduced the ability of Crl to interact with σ^S (Figure 4B and [16]). Residue Phe^{53} starts the β2-strand and might be important for the correct conformation of the protein. Arg^{51} is not involved in intra-molecular interactions and its side chain is oriented towards the outside of the molecule, making it a likely candidate for direct interaction with σ^S.

Finally, three conserved residues (Trp^{57}, Gly^{80}, Trp^{82}) form the hydrophobic patch 3 (Figure 5E), in which Gly^{80} belongs to loop 3 and Trp^{57} and Trp^{82} are located in the β2 and β4-strands, respectively. The substitution $Gly^{80}Ala$ did not affect the σ^S-Crl_{STM} interaction and Crl activity [16], whereas substitutions $Trp^{82}Ala$ and $Trp^{57}Ala$ had mild effects on the activity of Crl_{STM} *in vivo* and its ability to bind σ^S in BACTH experiments [16]. Residues Trp^{57} and Trp^{82} make stacking contacts, likely contributing to the structural stability of Crl. Consistent with this finding, Crl_{STM} variants $Trp^{82}Ala$ and $Trp^{57}Ala$ showed a high propensity to aggregate *in vitro* (data not shown). Therefore, these residues might be involved in maintaining the overall conformation of Crl rather than directly interacting with σ^S.

Altogether, these results pointed to conserved residues in Patch 1 and Patch 2 as potential candidates for direct interaction with σ^S and more specifically to the charged residues Asp^{36} and Arg^{51}, consistent with ITC results suggesting that complex formation is driven by electrostatic interactions. The substitutions $Arg^{51}Ala$ and $Asp^{36}Ala$ strongly affected also the interaction between Crl_{PM} and $\sigma^S{}_{STM}$, in agreement with data obtained for Crl_{STM}, whereas $Arg^{24}Ala$ had only a minor effect (Figure 4B). Furthermore, substitutions $Asp^{36}Ala$ and $Arg^{51}Ala$ abolished Crl_{STM} activity *in vivo* (Figure 4C,D). The lack of interaction of these Crl_{STM} variants with $\sigma^S{}_{STM}$ was further confirmed *in vitro* by SPR and ITC experiments (Figure S9A). The absence of binding of these Crl variants to σ^S might be due to the substitution of key residues directly involved in electrostatic interactions with σ^S or to conformational effects. To discriminate between these two possibilities, a biophysical characterization of these variants was undertaken (Figure 6). Crl_{STM} $Arg^{51}Ala$ showed structural features similar to those of wild-type Crl_{STM}, and thus that the lack of interaction with σ^S is due to the substitution of a residue directly involved in σ^S binding. In the case of the Crl_{STM} $Asp^{36}Ala$ variant, it is more difficult to draw a definite conclusion since the $Asp^{36}Ala$ substitution decreases the secondary and tertiary structural content of the protein with respect to wild-type Crl_{STM} (Figure 6A,B). These results were in line with DSC thermograms (Figure 6C) that showed a lower transition enthalpy for the Crl_{STM} $Asp^{36}Ala$ variant, whilst Crl_{STM} $Arg^{51}Ala$ had a similar transition enthalpy to wild-type Crl_{STM} ($\Delta H = 35.0 \pm 0.4$ kcal mol^{-1}). It must be emphasized, however that even though the conformation of Crl_{STM} $Asp^{36}Ala$ was affected *in vitro*, the level of production of this variant was not affected in the *S.* Typhimurium strain in physiological conditions, indicating that the protein was not unstable (Figure 4D). Asp^{36} establishes a salt bridge with Arg^{24} and makes hydrogen bonds with the side chain of Trp^{82} in

patch 3. This interaction network between the bottom of the cavity, loop 1 and loop 3 could play a role in controlling the size of the cavity. The loss of these Asp^{36}-mediated interactions could also explain the structural changes observed in the Crl_{STM} $Asp^{36}Ala$ variant (Figure 6). On the other hand, direct interaction between Asp^{36} and σ^S might affect the intra-molecular network involving Asp^{36} and this might, in turn, trigger a conformational change in Crl. Whether conformational changes in Crl occur upon σ^S binding and whether they affect the stability of the complex is an interesting issue for future studies. Additional experiments are underway to characterize in more detail the possible interaction networks involving Asp^{36}, both within Crl and between Crl and σ^S. It is worth noting that albeit our study focussed on the role of conserved Crl residues involved in σ^S binding, non-conserved residues might affect the global affinity of Crl for σ^S. Indeed, the σ^S binding region of Crl corresponds to a cavity enclosed by flexible loops/arms. The non-conserved residues in the Crl loops might differentially modulate the flexibility of the arms, thus controlling the capacity of Crl from different species to interact with σ^S. This might result in the higher affinity of Crl_{PM} observed for full-length σ^S and $\sigma^S_{53\text{-}162}$ with respect to Crl_{STM}. Our future studies will focus on the functional role of the flexible loops in the Crl structure for the recognition and binding to σ^S and on the identification of the structural interface between Crl and domain 2 of σ^S.

CONCLUSION

So far, Crl is the only known factor able to bind σ^S and increase its affinity for the core RNAP [11, 13-15]. Since σ^S is widespread in bacteria and well conserved at the sequence level, the narrow distribution of Crl among proteobacteria and its lower level of sequence conservation with respect to σ^S might be surprising at first glance. Regulation of σ^S activity might have evolved in bacteria that do not contain *crl* to adapt to the specific lifestyle of bacteria and/or there might be functional homologues of Crl in these species. Our results with the Crl proteins from *P. mirabilis* (this study) and *Vibrio cholerae* (data not shown) suggest that Crl family members interact with σ^S and are functional. The overall tertiary structure of Crl is likely retained, with small differences that may result from local structural changes in the flexible loops present in the Crl structure. These loops may have dynamic roles in the recognition and binding mechanism of σ^S, as well as in the stability and/or regulation of Crl activity.

Experiments using bacterial two-hybrid systems demonstrated that σ^S domain 2 interacts with Crl proteins from *S.* Typhimurium [20], *E. coli* [14] and *P. mirabilis* (this study). In the present study, we further show that purified σ^S domain 2 (residues 52-162) accounts for the affinity and kinetics of interaction of full-length σ^S with Crl_{STM} and Crl_{PM}. An interesting feature of the complex between Crl and either full-length σ^S or its domain 2 alone, is its short lifetime. This on-off mechanism is likely to be important in the process of σ^S activation and binding to the RNA polymerase, but its molecular basis is unknown. The flexibility of Crl might be a key feature, with Crl intrinsic dynamics controlling the association and dissociation steps. This dynamic behaviour may also be a key feature of the potential regulation of Crl activity by environmental signals, allowing bacteria to adjust Crl affinity for σ^S as needed.

In this study, we identified in the Crl structure a cavity enclosed by flexible loops, containing surface-exposed residues important for the interaction with σ^S and conserved in Crl-family members. One of these residues, Arg^{51}, is directly involved in the binding of σ^S, whereas Asp^{36} may establish a direct interaction with σ^S and/or contribute to conformational changes of Crl. A recent study in *E. coli* identified two areas in domain 2 of σ^S required for Crl binding [14]. This finding and the identification in this study of Crl structural patches and key residues involved in σ^S binding will facilitate the future delimitation of the Crl-σ^S interface.

ACCESSION NUMBERS

Atomic coordinates and structure factors of Crl *Proteus mirabilis* have been deposited with the RCSB PDB with the entry code **4Q11.**

ACKNOWLEDGEMENT

We thank A. Pugsley and all members of the laboratory for their kind support. We are grateful to M. Nowakowski for protein production and helping in the purification of the proteins used, and E. Frachon for bioreactor cultures. We acknowledge B. Baron and S. Hoos for assistance with the biophysical assays. We thank C. Romier for providing vectors pET-MCN-EAVNH and pET-MCN-YC. We are also grateful to M. E. Shirtiff and H. Mobley for providing *P. mirabilis* HI4320 and D. Ladant for the T25 antibody. We acknowledge SOLEIL for provision of synchrotron radiation facilities and would like to thank the staff of beamline PROXIMA-1 for assistance.

FUNDING

This work was supported by the French National Research Agency [grant ANR- 11-BSV3-009] and by grants from the Institut Pasteur and the Centre National de la Recherche Scientifique.

REFERENCES

1 Lee, D. J., Minchin, S. D. and Busby, S. J. (2012) Activating transcription in bacteria. Annu Rev Microbiol **66**, 125-152

2 Gruber, T. M. and Gross, C. A. (2003) Multiple sigma subunits and the partitioning of bacterial transcription space. Annu Rev Microbiol **57**, 441-66

3 Österberg, S., del Peso-Santos, T. and Shingler, V. (2011) Regulation of alternative sigma factor use. Annu Rev Microbiol **65**, 37-55

4 Battesti, A., Majdalani, N. and Gottesman, S. (2011) The RpoS-mediated general stress response in *Escherichia coli*. Annu Rev Microbiol **65**, 189-213

5 Hengge, R. (2011) The general stress response in Gram-negative bacteria, Bacterial Stress Responses (Second Edition, eds. G. Storz and R. Hengge), ASM Press, Washington D.C.

6 Ishihama, A. (2000) Functional modulation of *Escherichia coli* RNA polymerase. Annu Rev Microbiol **54**, 499-518

7 Klauck, E., Typas, A. and Hengge, R. (2007) The sigmaS subunit of RNA polymerase as a signal integrator and network master regulator in the general stress response in *Escherichia coli*. Sci Prog **90**, 103-27

8 Pratt, L. A. and Silhavy, T. J. (1998) Crl stimulates RpoS activity during stationary phase. Mol Microbiol **29**, 1225-36

9 Bougdour, A., Lelong, C., Geiselmann, J. (2004) Crl, a low temperature-induced protein in *Escherichia coli* that binds directly to the stationary phase σ subunit of RNA polymerase J Biol Chem **279**, 19540-19550

10 Gaal, T., Mandel, M. J., Silhavy, T. J. and Gourse, R. L. (2006) Crl facilitates RNA polymerase holoenzyme formation. J Bacteriol **188**, 7966-70

11 Robbe-Saule, V., Jaumouille, V., Prevost, M. C., Guadagnini, S., Talhouarne, C., Mathout, H., Kolb, A. and Norel, F. (2006) Crl activates transcription initiation of RpoS-regulated genes involved in the multicellular behavior of *Salmonella enterica* serovar Typhimurium. J Bacteriol **188**, 3983-94

12 Robbe-Saule, V., Lopes, M. D., Kolb, A. and Norel, F. (2007) Physiological effects of Crl in *Salmonella* are modulated by sigmaS level and promoter specificity. J Bacteriol **189**, 2976-87

13 Typas, A., Barembruch, C., Possling, A. and Hengge, R. (2007) Stationary phase reorganisation of the *Escherichia coli* transcription machinery by Crl protein, a fine-tuner of σ^S activity and levels. EMBO J **26**, 1569-1578

14 Banta, A. B., Chumanov, R. S., Yuan, A. H., Lin, H., Campbell, E. A., Burgess, R. R. and Gourse, R. L. (2013) Key features of sigmaS required for specific recognition by Crl, a transcription factor promoting assembly of RNA polymerase holoenzyme. Proc Natl Acad Sci U S A **110**, 15955-15960

15 England, P., Westblade, L. F., Karimova, G., Robbe-Saule, V., Norel, F. and Kolb, A. (2008) Binding of the unorthodox transcription activator, Crl, to the components of the transcription machinery. J Biol Chem **283**, 33455-64

16 Monteil, V., Kolb, A., D'Alayer, J., Beguin, P. and Norel, F. (2010) Identification of conserved amino acid residues of the *Salmonella* sigmaS chaperone Crl involved in Crl-sigmaS interactions. J Bacteriol **192**, 1075-87

17 Lonetto, M., Gribskov, M. and Gross, C. A. (1992) The sigma 70 family: sequence conservation and evolutionary relationships. J Bacteriol **174**, 3843-9

18 Murakami, K. S. and Darst, S. A. (2003) Bacterial RNA polymerases: the wholo story. Curr Opin Struct Biol **13**, 31-9

19 Paget, M. S. and Helmann, J. D. (2003) The sigma70 family of sigma factors. Genome Biol **4**, 203
20 Monteil, V., Kolb, A., Mayer, C., Hoos, S., England, P. and Norel, F. (2010) Crl binds to domain 2 of sigma(S) and confers a competitive advantage on a natural *rpoS* mutant of *Salmonella enterica* serovar Typhi. J Bacteriol **192**, 6401-10
21 Schmieger, H. (1972) Phage P22-mutants with increased or decreased transduction abilities. Mol Gen Genet **119**, 75-88
22 Sternberg, N. L. and Maurer, R. (1991) Bacteriophage-mediated generalized transduction in *Escherichia coli* and *Salmonella typhimurium*. Methods Enzymol **204**, 18-43
23 Sambrook, J., Fritsch, E. F. and Maniatis, T. (1989) Molecular cloning: a laboratory manual, 2nd ed, Cold Spring Harbor Laboratory Press, Cold Spring Harbor, NY
24 Bochner, B. R., Huang, H. C., Schieven, G. L. and Ames, B. N. (1980) Positive selection for loss of tetracycline resistance. J Bacteriol **143**, 926-33
25 Datsenko, K. A. and Wanner, B. L. (2000) One-step inactivation of chromosomal genes in *Escherichia coli* K-12 using PCR products. Proc Natl Acad Sci U S A **97**, 6640-5
26 Gerlach, R. G., Jackel, D., Holzer, S. U. and Hensel, M. (2009) Rapid oligonucleotide-based recombineering of the chromosome of *Salmonella enterica*. Appl Environ Microbiol **75**, 1575-80
27 Karimova, G., Pidoux, J., Ullmann, A. and Ladant, D. (1998) A bacterial two-hybrid system based on a reconstituted signal transduction pathway. Proc Natl Acad Sci U S A **95**, 5752-6
28 Miller, J. H. (1972) Experiments in molecular genetics, Cold Spring Harbor Laboratory Press, Cold Spring Harbor, NY
29 Kabsch, W. (2010) Xds. Acta Crystallogr D Biol Crystallogr **66**, 125-32
30 Winn, M. D., Ballard, C. C., Cowtan, K. D., Dodson, E. J., Emsley, P., Evans, P. R., Keegan, R. M., Krissinel, E. B., Leslie, A. G., McCoy, A., McNicholas, S. J., Murshudov, G. N., Pannu, N. S., Potterton, E. A., Powell, H. R., Read, R. J., Vagin, A. and Wilson, K. S. (2011) Overview of the CCP4 suite and current developments. Acta Crystallogr D Biol Crystallogr **67**, 235-42
31 McCoy, A. J., Grosse-Kunstleve, R. W., Adams, P. D., Winn, M. D., Storoni, L. C. and Read, R. J. (2007) Phaser crystallographic software. J Appl Crystallogr **40**, 658-674
32 Murshudov, G. N., Skubák, P., Lebedev, A. A., Pannu, N. S., Steiner, R. A., Nicholls, R. A., Winn, M. D., Long, F. and Vagin, A. (2011) REFMAC5 for the refinement of macromolecular crystal structures. Acta Crystallogr D Biol Crystallogr **67**, 355-367
33 Emsley, P., Lohkamp, B., Scott, W. G. and Cowtan, K. (2010) Features and development of Coot. Acta Crystallogr D Biol Crystallogr **66**, 486-501
34 Sali, A., Potterton, L., Yuan, F., van Vlijmen, H. and Karplus, M. (1995) Evaluation of comparative protein modelling by MODELLER. Proteins **23**, 318-326
35 McGuffin, L., J.,, Buenavista, M. T. and Roche, D. B. (2013) The ModFOLD4 Server Quality Assessment of 3D Protein Models. Nucleic Acids Res **41**, W368-W372
36 Zhang, Y. and Skolnick, J. (2005) TM-align: A protein structure alignment algorithm based on TM-score. Nucleic Acids Res **33**, 2302-2309
37 Krissinel, E. and Henrick, K. (2007) Inference of molecular assemblies from crystalline state. J. Mol. Biol **372**, 774-797
38 Callaci, S., Heyduk, E. and Heyduk, T. (1999) Core RNA polymerase from *E. coli* induces a major change in the domain arrangement of the sigma 70 subunit. Mol Cell **3**, 229-38

39 Romling, U. (2005) Characterization of the rdar morphotype, a multicellular behaviour in Enterobacteriaceae. Cell Mol Life Sci **62**, 1234-46

TABLE LEGEND

Table 1. Thermodynamic parameters of the interaction of σ^S_{STM} with both Crl_{PM} and Crl_{STM} obtained by ITC at 25°C
Each ITC experiment was performed in triplicate and standard deviations are reported.

	n	K_D (μM)	$\Delta_b H$ (kJ/mol)	$T\Delta_b S$ (kJ/mol)	$\Delta_b G$ (kJ/mol)
σ^S_{STM} + Crl_{STM}	1.0 ± 0.1	0.8 ± 0.2	-8.2 ± 0.5	27 ± 1	-35 ± 1
σ^S_{STM} + Crl_{PM}	0.98 ± 0.07	0.4 ± 0.1	-5.9 ± 0.7	30 ± 1	-36 ± 1

FIGURE LEGENDS

Figure 1. X-ray crystal structure of Crl_{PM} (4Q11)
(A) Cartoon representation of the Crl_{PM} dimer with an interface of 987 $Å^2$. The cavity formed by the β-strand bed and the flexible loops are indicated for one monomer of the asymmetric unit. **(B)** Single Crl_{PM} monomer showing the α1α2β1β2β3β4β5α3β6α4 architecture and the three flexible loops. **(C)** B-factor representation of Crl_{PM}. The loops 1 and 2 possess the highest temperature factor values.

Figure 2. Interaction between Crl and σ^S proteins from *S.* Typhimurium and *P. mirabilis* in the BACTH assay
(A) Interaction between the indicated hybrid proteins was quantified by measuring β-galactosidase activity in *E. coli* DHT1 cells. Results are the mean of at least three independent experiments and standard deviations are indicated with black bars. **(B)** Immunodetection of T25-σ^S and Crl-T18 hybrid proteins using antibodies directed against T25 and T18, respectively. Lane 1: T25-unfused, lane 2: T25-σ^S_{STM}, lane 3: T25-σ^S_{PM}, lane 4: unfused-T18, lane 5: Crl_{STM}-T18, lane 6: Crl_{PM}-T18.

Figure 3. SPR binding analysis of Crl_{STM} and Crl_{PM} to full-length σ^S_{STM} and its domain 2 ($\sigma^S_{53\text{-}162}$).
Association and dissociation real time profiles corresponding to the interaction of immobilised $(his)_6$-σ^S_{STM} with Crl_{STM} **(A)** and of $(his)_6$-$\sigma^S_{53\text{-}162}$ with either Crl_{STM} **(B)** or Crl_{PM} **(C)**. The following Crl concentrations were used: 123 nM (black), 370 nM (pink), 1.1 μM (red), 3.3 μM (green), 10 μM (blue). In inset are shown the steady state response curves as a function of Crl protein concentration.

Figure 4. Functional analyses of Crl variants *in vivo*
Rdar morphotype of *S.* Typhimurium strains harboring the heterologous crl_{PM} allele **(A)** and the crl_{STM} mutated alleles producing the Asp^{36}Ala and Arg^{51}Ala Crl_{STM} variants **(C)**. The wild-type strain ATCC14028 (WT) and its *ΔrpoS* and Δ*crl* derivatives were used as controls. **(B)** BACTH experiments with T25-σ^S_{STM} and the Crl-T18 hybrid proteins from *S.* Typhimurium and *P. mirabilis* carrying the indicated alanine substitutions. Interactions were quantified by measuring β-galactosidase activity. Results are the mean of at least three independent experiments and standard deviations are indicated with black bars. **(D)** Immunodetection of Crl_{STM}-T18 fusion proteins using antibody directed against T18 and of the Crl_{STM} variant proteins expressed in *S.* Typhimurium ATCC14028 (panel C) using an anti-Crl_{STM} antibody.

Figure 5. Structural homology model of Crl_{STM} based on the X-ray crystal structure of Crl_{PM} (4Q11)
(A,B) Cartoon and surface representation of the Crl_{STM} model in which are shown the conserved residues of the Crl family members [16] forming three patches of surface-exposed residues. Zoomed views of residues belonging to patch 1 **(C)**, patch 2 **(D)** and patch 3 **(E)**. In patch 1, D36 establishes a salt bridge with R24 (distance between Asp^{36} $O_{δ1}$ and Arg^{24} Nε atoms of about 2.6 Å and 3.3 Å and between Asp^{36} $O_{δ2}$ and Arg^{24} $N_ν$ atoms of about 3.2 and 2.7 in 4Q11 and Crl_{STM} model, respectively) and a hydrogen bond with Trp^{82} (distance between Asp^{36} $O_{δ2}$ and Trp^{82} Nε atoms of about 2.8 Å and 3.3 Å in 4Q11 and Crl_{STM} model, respectively).

Figure 6. Structural and thermal stability characterization of the Crl_{STM} Asp^{36}Ala and Crl_{STM} Arg^{51}Ala variants

(A) Far-UV (200-260 nm) and near-UV (260-320 nm) CD spectra. **(B)** Fluorescence spectra recorded at an excitation wavelength of 280 nm (solid line) and 295 nm (dotted line). **(C)** DSC thermograms obtained at a scan rate of 200 °C/hour from 10 to 80 °C. The transition temperature and enthalpy for Crl_{STM} $Asp^{36}Ala$ were 60 ± 1 °C and ΔH = 16.5 ± 0.2 kcal mol^{-1}, respectively, and for Crl_{STM} $Arg^{51}Ala$ were 59 ± 1 °C and ΔH = 31.6 ± 0.2 kcal mol^{-1}. In all panels, wild-type Crl_{STM} is represented by solid lines, Crl_{STM} $Asp^{36}Ala$ by dotted lines and Crl_{STM} $Arg^{51}Ala$ by dashed lines.

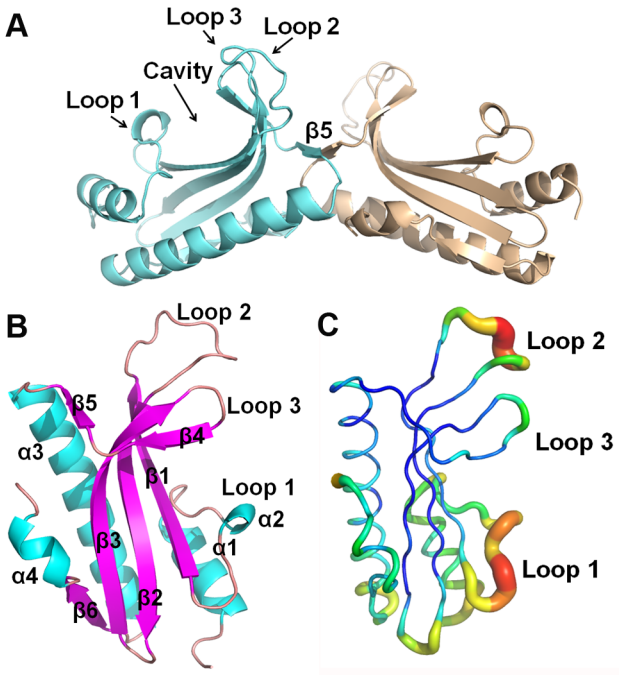
A
Loop 3
Loop 2
Cavity
Loop 1
β5
B
Loop 2
β5
Loop 3
β4
α3
β1
Loop 1
α2
β3
α1
α4
β6
β2
C
Loop 2
Loop 3
Loop 1

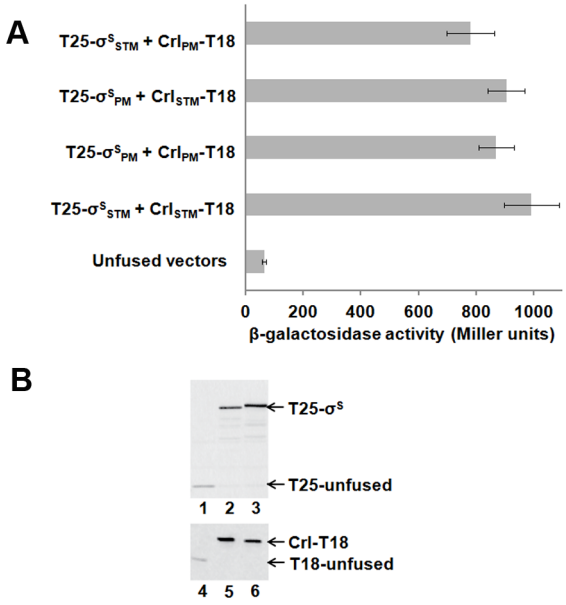
A
T25-σ^S_STM + CrI_PM-T18
T25-σ^S_PM + CrI_STM-T18
T25-σ^S_PM + CrI_PM-T18
T25-σ^S_STM + CrI_STM-T18
Unfused vectors
0
200
400
600
800
1000
β-galactosidase activity (Miller units)
B
T25-σ^S
T25-unfused
1 2 3
CrI-T18
T18-unfused
4 5 6

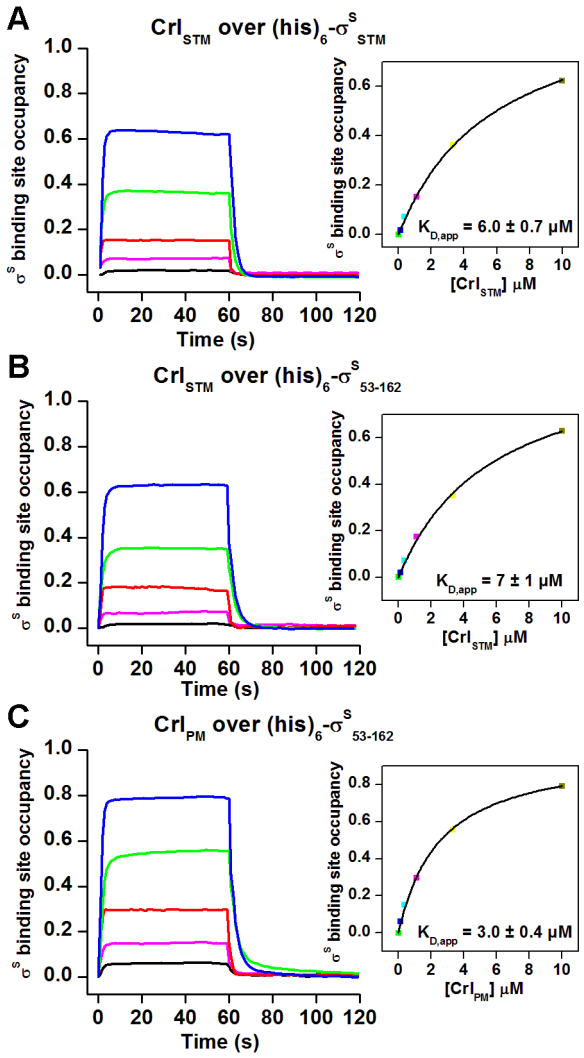
A
Crl STM over (his)6-σS STM
σS binding site occupancy
Time (s)
KD,app = 6.0 ± 0.7 μM
[Crl STM] μM
B
Crl STM over (his)6-σS 53-162
KD,app = 7 ± 1 μM
C
Crl PM over (his)6-σS 53-162
KD,app = 3.0 ± 0.4 μM
[Crl PM] μM

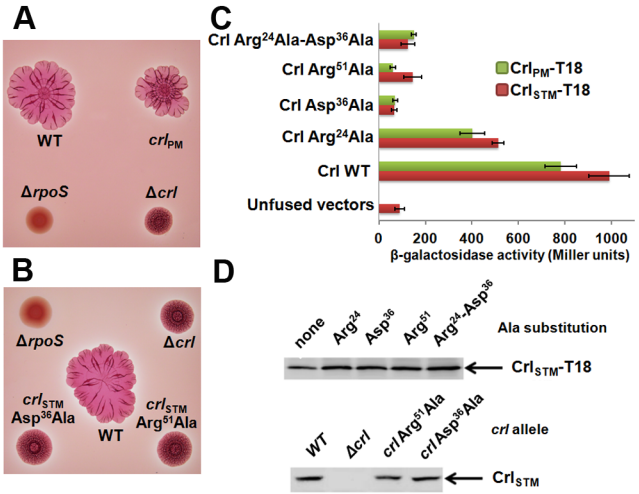
A
WT
crlPM
ΔrpoS
Δcrl
B
ΔrpoS
Δcrl
crlSTM Asp36Ala
WT
crlSTM Arg51Ala
C
Crl Arg24Ala-Asp36Ala
Crl Arg51Ala
Crl Asp36Ala
Crl Arg24Ala
Crl WT
Unfused vectors
CrlPM-T18
CrlSTM-T18
β-galactosidase activity (Miller units)
D
none
Arg24
Asp36
Arg51
Arg24-Asp36
Ala substitution
CrlSTM-T18
WT
Δcrl
crlArg51Ala
crlAsp36Ala
crl allele
CrlSTM

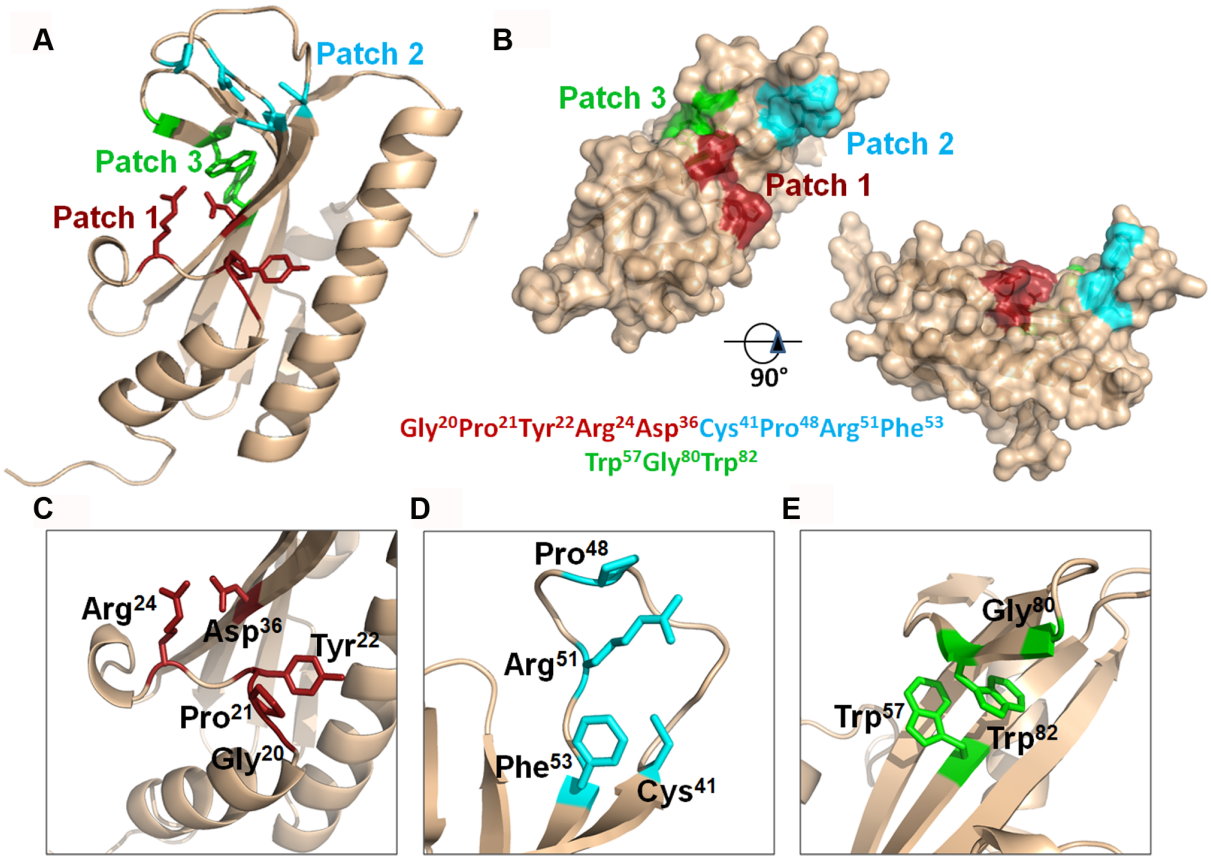
A
Patch 2
Patch 3
Patch 1
B
Patch 3
Patch 2
Patch 1
90°
Gly20Pro21Tyr22Arg24Asp36Cys41Pro48Arg51Phe53
Trp57Gly80Trp82
C
Arg24
Asp36
Tyr22
Pro21
Gly20
D
Pro48
Arg51
Phe53
Cys41
E
Gly80
Trp57
Trp82

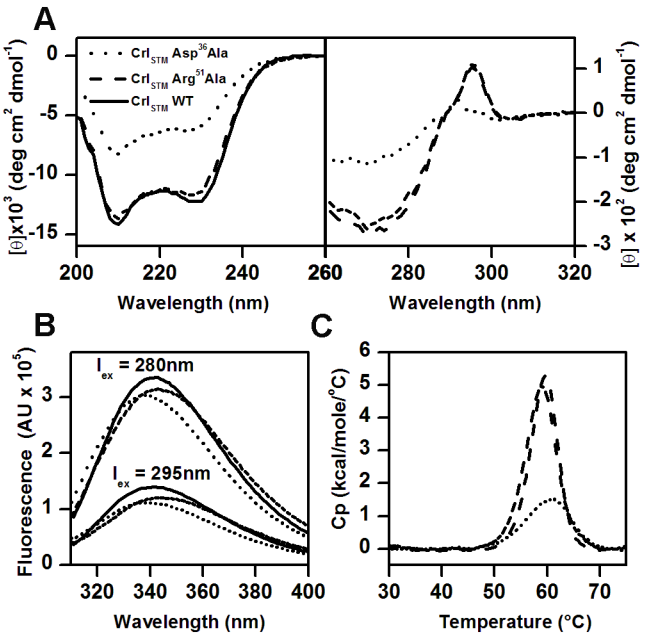
A
CrlSTM Asp36Ala
CrlSTM Arg51Ala
CrlSTM WT
[θ]x10³ (deg cm² dmol⁻¹)
[θ] x 10² (deg cm² dmol⁻¹)
Wavelength (nm)
Wavelength (nm)
B
Iex = 280nm
Iex = 295nm
Fluorescence (AU x 10⁵)
Wavelength (nm)
C
Cp (kcal/mole/°C)
Temperature (°C)